Photodiagnosis and Photodynamic Therapy 38 (2022) 102863

Contents lists available at ScienceDirect

Photodiagnosis and Photodynamic Therapy

journal homepage: www.elsevier.com/locate/pdpdt

# Novel cationic-chalcone phthalocyanines for photodynamic therapy eradication of *S. aureus* and *E. coli* bacterial biofilms and MCF-7 breast cancer

Yolande Ikala Openda *, Balaji Babu, Tebello Nyokong *

*Institute for Nanotechnology Innovation, Rhodes University, Makhanda 6140, South Africa*

ARTICLE INFO

*Keywords:*
Cationic phthalocyanines
*S. aureus*
*E. coli*
Biofilms
Photodynamic antimicrobial therapy
MCF-7 breasts cancer cells
Photodynamic Therapy

ABSTRACT

New tetrasubstituted zinc (II) and indium (III) phthalocyanines bearing dimethylamino chalcone group (complexes **3** and **4)** as well as their quaternized analogs (**3a** and **4a**) have been assessed for their photodynamic therapy (PDT) of cancer as well as photodynamic antimicrobial chemotherapy activities against biofilms and planktonic cultures of pathogenic bacteria of *Staphylococcus aureus* and *Escherichia coli*. Compared to the non-quaternized phthalocyanines **3** and **4**, the cationic phthalocyanines **3a** and **4a** exhibit a higher photodynamic inactivation against the planktonic cells with log reduction values above 9 at a concentration of 1.25 μM. This was attributed to the positive charge which enhances cellular uptake. More interestingly, **3a** and **4a** show a higher photodynamic inactivation (less than 3% of *S. aureus* survived) on their biofilm counterparts thanks to their stronger affinity to these cells. **3a** and **4a** Pcs also exhibited interesting PDT activity against MCF-7 cancer cells giving $IC_{50}$ values of 17.9 and 7.4 μM, respectively following 15 min irradiation. The obtained results in this work show that the positively charged phthalocyanines **3a** and **4a** are potential antibacterial photosensitizers that show some selectivity toward the Gram-positive and Gram-negative bacteria as well as MCF-7 breasts cancer cells.

## 1. Introduction

Light energy targeting techniques such as photodynamic therapy (PDT) of cancer [1,2] and photodynamic antimicrobial chemotherapy (PACT) for microbes [3] are being investigated as the most advanced and effective curative approaches that could overcome the limitations of conventional therapies such as chemotherapy. For instance, in PACT multiple and alternative sites in the bacteria cell are targeted, hence making it a promising method for the eradication of microbes with no possibility of them developing drug resistance [3–7] while PDT has been also proven to be non-invasive with fewer side effects with little systemic toxicity [1,8–10].

In PACT as in PDT, a light source of appropriate wavelength is used to irradiate a nontoxic photosensitizer which will generate reactive oxygen species (ROS) including singlet oxygen that can exert a bactericidal effect on planktonic [11–13] or biofilm [14,15] cultures of pathogenic bacteria. In PDT, the ROS can cause localized necrosis to the target cancerous cells without damaging the host tissue [16,17].

Since the therapeutic efficacy of PACT and PDT largely depends on the photochemical and photobiological properties of the photosensitizer being used; an ideal photosensitizer for PACT/PDT should be able to attach to the cell wall and/or accumulate inside the target cell without causing any damage to the normal cells. For this reason, the use of positively charged drugs is required as they show enhanced water solubility and cellular uptake efficiency, thereby increasing their antimicrobial or anticancer potency [18,19].

Chalcones are vascular disrupting compounds known to destroy the tumors' neovasculature, therefore, inducing tumor death by necrosis [20]. This group of compounds lessens the problem of hypoxia, a pathological phenomenon in which tissues are starved of adequate oxygen [21]. Our recent work reported on the enhanced antimicrobial photo-ablation effect of chalcone-derived phthalocyanines conjugated to detonation nanodiamonds [22]. This report encouraged us to combine phthalocyanines (Pcs), which are excellent PACT/PDT photosensitizers due to their near-infrared maximal absorption and high singlet oxygen generation ability [23] with dimethylamino-chalcone as the substituent, to form tetrasubstituted zinc and indium Pcs and their quaternized (positively charged) Pc analogs. Thus, in this work, we

* Corresponding author.
*E-mail addresses:* yolandeopenda@gmail.com (Y.I. Openda), t.nyokong@ru.ac.za (T. Nyokong).

https://doi.org/10.1016/j.pdpdt.2022.102863
Received 17 February 2022; Received in revised form 6 April 2022; Accepted 12 April 2022
Available online 14 April 2022
1572-1000/

employ a bulkier chalcone substituent for the Pcs and apply them for both PDT and PACT. The dimethylamino chalcone groups will result in the Pcs being bulky hence preventing aggregation. This approach aims to produce photosensitizer agents with complementary antimicrobial and anticancer properties that can strongly inhibit both Gram-positive and Gram-negative planktonic and biofilm cultures of pathogenic bacteria as well as the MCF-7 breast cancer cells using a photodynamic process. These strategies have been reported to be safe and reliable for the successful reduction of the burden caused by biofilm formation in chronic infections [24] and breast cancer which constitutes one of the most common causes of cancer-leading death in women [25].

## 2. Experimental

### 2.1. Materials

All reactions were carried out under an inert atmosphere of argon. 4-Hydroxyacetophenone, 4-dimethylaminobenzaldehyde, 4-nitrophthalonitrile, potassium hydroxide, potassium carbonate, anhydrous zinc (II) acetate ($(ZnOAc)_2$), anhydrous indium (III) chloride iodomethane, diphenylisobenzofuran (DPBF), anthracene-9,10-bis-methylmalonate (ADMA), 1,8-diazabicyclo[5.4.0]undec-7-ene (DBU), deuterated dimethyl sulfoxide (DMSO-*d6*), pentanol, and crystal violet were acquired from Sigma Aldrich. Some solvents such as dimethyl sulfoxide (DMSO), *N,N*-dimethylformamide (DMF), ethanol, and acetone were purchased from Merck. Other reagents and solvents were obtained from commercial suppliers and were of analytical grade and used without any further purification. Phosphate-buffered saline (PBS) solution pH 7.4 was prepared using appropriate amounts of $Na_2HPO_4$ and $KH_2PO_4$ in ultra-pure water from ELGA, Veolia PURELAB, flex system (Marlow, UK). ClAlPcSmix (mixture of Aluminum sulfonated Pcs derivatives) was synthesized according to literature methods [26].

Nutrient agar, agar broth, and agar bacteriological BBL Mueller Hinton broth were purchased from Merck and prepared as specified by the suppliers. *Staphylococcus aureus* (ATCC) and *Escherichia coli* (ATCC) were obtained from Davies Diagnostics while MCF-7 breast cancer cells were acquired from Cellonex. Dulbecco's phosphate-buffered saline (DPBS) and Dulbecco's modified Eagle's medium (DMEM) were obtained from Lonza, 10% (v/v) heat-inactivated fetal calf serum (FCS) and 100 mg per mL-penicillin-100 unit per mL-streptomycin-amphotericin B mixture were obtained from Biowest®.

### 2.2. Equipment

A Shimadzu UV-2250 spectrophotometer and a Varian Eclipse spectrofluorimeter were used to record all the ground state absorption and fluorescence spectra in solution, respectively. Time correlation single photon counting (TCSPC) equipped with a Picoquant GmbH containing a LDH-P-670 diode laser with a 44 ps pulse width and 20 MHz rate repetition was used to determine fluorescence lifetimes for all complexes. Singlet oxygen quantum yield determination was carried out in a general electric Quartz line projector lamp combined with a 600 nm cut-off filter along with a water filter. An additional interference filter (Intor, 670 nm having a bandwidth of 40 nm) was aligned before the sample. $^{1}H$ and $^{13}C$ NMR measurements in deuterated DMSO were performed using a Bruker® AVANCE 600 MHz NMR spectrometer. A Bruker AutoFLEX III Smartbeam MALDI-TOF mass spectrometer was employed for the recording of mass spectra. Infrared spectroscopy was performed using a Bruker Alpha IR (100 FT-IR) spectrophotometer with universal attenuated total reflectance (ATR). Energy-dispersive X-ray spectrometer (EDX, INCA PENTA FET coupled with VAGA TESCAM operated at 20 kV) was utilized to qualitatively determine the elemental compositions of the studied complexes. Elemental analyses were performed using a Vario-Elementar Microcube ELIII. A Metrohm Swiss 827 pH meter was used for pH measurements. HERMLE Z233M-2 centrifuge was used for the harvesting of the bacteria cells. PRO VSM-3 Labplus Vortex mixer was used for the homogenization of the bacteria suspension. A thermostatic oven was used for incubation processes. The optical density of the bacteria was determined using the LEDETECT 96. Scan® 500 automatic color colony counter was used to evaluate the colony forming units CFU/mL of the bacteria. Irradiation for PACT and PDT studies was conducted using Modulight® Medical Laser System (MLS) 7710–670 channel Turnkey laser system coupled with a 2.3 W channel at 670 nm (with irradiation doses of 170 J.cm$^{-2}$) cylindrical out-put channels, aiming beam, an integrated calibration module, foot/hand switch pedal, sub-miniature version A connectors, and safety interlocks were used. The illumination kit for in vitro PDT studies can hold 127.76 x 85.48 mm 96 well tissue culture plates.

### 2.3. Synthesis

#### 2.3.1. (E)−3-(4-(dimethylamino)phenyl)−1-(4-hydroxyphenyl)prop-2-en-1-one (1), scheme 1

The chalcone compound (**1**) was prepared according to the Claisen-Schmidt condensation procedure with slight modifications (Scheme 1) [27,28]. Briefly, 4-hydroxyacetophenone (1 g, 7.3 mmol) and 4-dimethylaminobenzaldehyde (1.096 g, 7.3 mmol) were dissolved in ethanol (20 mL) and the mixture was added dropwise to a stirred solution of 40% KOH, followed by cooling at 0 °C in an ice bath under argon atmosphere.

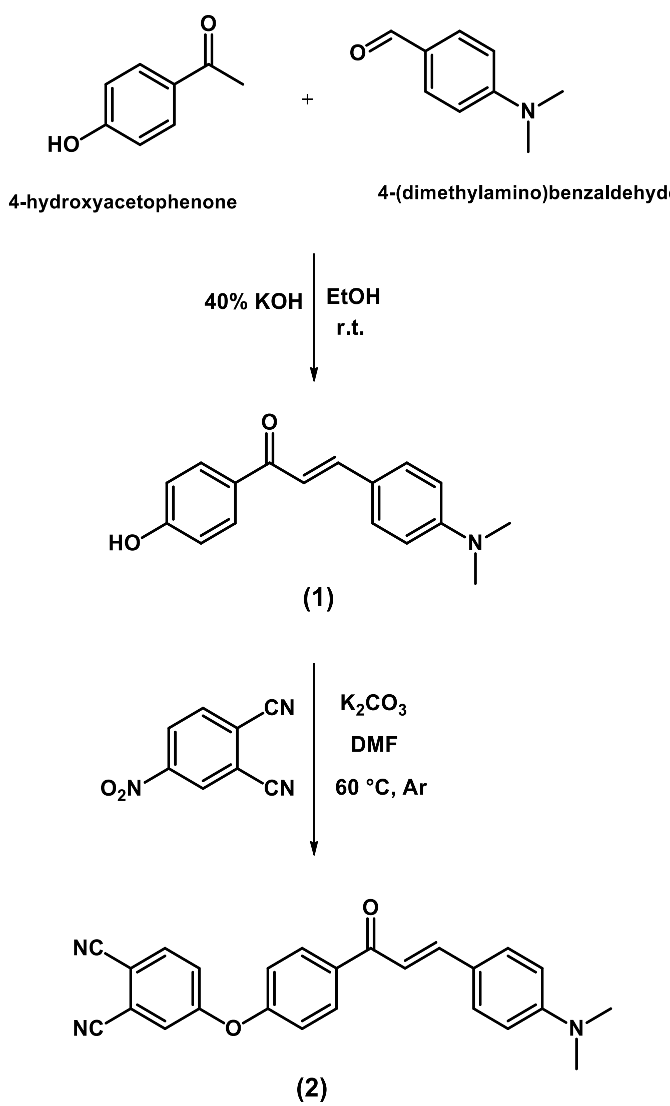


**Scheme 1.** Synthetic pathways of chalcone (**1**) and chalcone-derived phthalonitrile (**2**).

The reaction mixture was left to stir at room temperature for 24 h and thin-layer chromatography (TLC) was used to check if the reaction was complete. Once done, the reaction mixture was poured into ice water and 1 M HCl was used to adjust the mixture to neutral pH to precipitate out the desired product which was then recrystallized using ethanol.

A yellow powder, yield: 72%. FT-IR (UATR-TWO™) $\nu$ max/cm$^{-1}$: 3094 (OH), 2805 (Ar C—H and intermolecular H bonds), 2710 (Alph C—H), 1663 (C = O), 1591 (C = C), 1536 (C = N), 1437–1356 (C—C). $^{1}$H NMR (600 MHz, DMSO- $d_6$): δ (ppm): 9.66 (bs, 1H, -OH), 8.01 (*d, J* = 8.4 Hz, 2H, Ar-H), 7.67 (*d, J* = 16.1 Hz, 1H, *trans*-H), 7.64 (*d, J* = 8.1 Hz, 2H, Ar-H), 6.86 (*d, J* = 8.1 Hz, 2H, Ar-H), 6.78 (*d, J* = 15.9 Hz, 1H, *trans*-H), 6.73 (*d, J* = 8.2 Hz, 2H, Ar-H) and 2.99 (*s*, 6H, N-($CH_3$)$_2$). $^{13}$C NMR (600 MHz, DMSO- $d_6$): δ (ppm): 190.5, 158.7, 136.9, 125.2, 125.2, 124.9, 121.3, 117.6, 116.2, 115.8, 111.5, 111.1 and 40.5.

*2.3.2. Synthesis of (E)−4-(4-(3-(4-(dimethylamino)phenyl)acryloyl) phenoxy)phthalonitrile (2), scheme 1*

A mixture of 4-nitrophthalonitrile (0.971 g, 5.6 mmol) and compound **1** (1 g, 3.7 mmol) and $K_2CO_3$ (0.775 g, 5.6 mmol) was dissolved in 20 mL of dry DMF and stirred under argon atmosphere for 24 h at 60 °C. The reaction was monitored using thin-layer chromatography (TLC). Following completion of the reaction, the product was precipitated out in ice water, then filtered while washing with water. The resulting solid was filtered out and recrystallized in ethanol to obtain **2**.

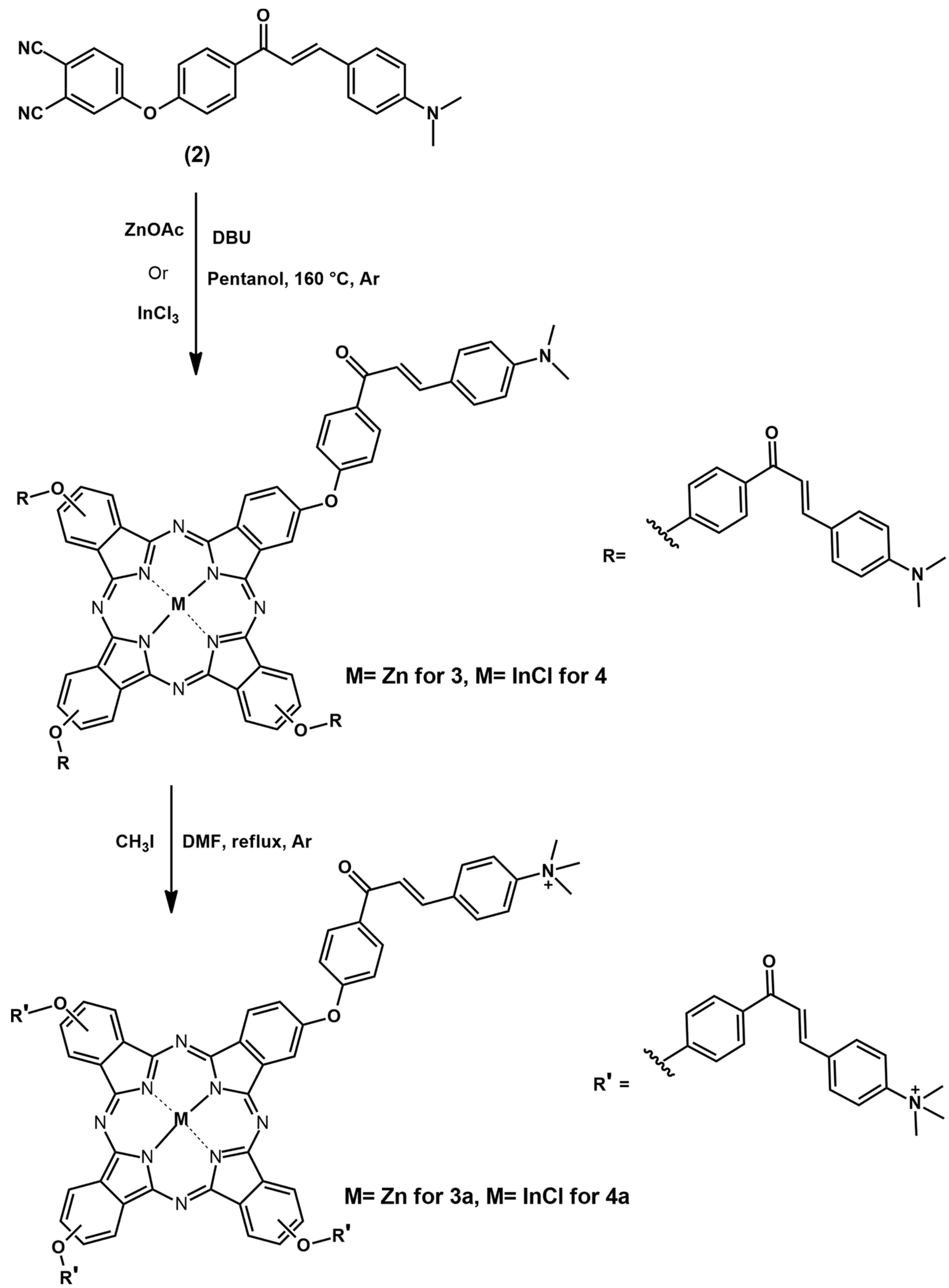


**Scheme 2.** Synthetic route of phthalocyanine complexes.

A light yellow solid. Yield: 85%. FT-IR (UATR-TWO™) ν max/cm$^{-1}$: 2911 (Ar C—H and intermolecular H bonds), 2806 (Aliph C—H), 1667 (C = O), 1588 (C = C), 1536 (C = N), 2225 (C≡N), 1477–1387 (C—C), 1299–1160 (*Asym.*, Ar-O-Ar), 1075 (*Sym.*, Ar-O-Ar), 812. $^1$H NMR (600 MHz, DMSO-$d_6$): δ (ppm): 7.87 (*d, J* = 8.2 Hz, 2H, Ar-H), 7.75 (*d, J* = 8.1 Hz, 2H, Ar-H dimethylamino), 7.73 (*s*, 1H, Ar-H), 7.64 (*d, J* = 15.8 Hz, 1H, *trans*-H), 7.57 (*d, J* = 8.2 Hz, 1H, Ar-H), 7.47 (*d, J* = 16.0 Hz, 1H, *trans*-H), 7.21 (*d, J* = 8.2 Hz, 2H, Ar-H), 7.17 (*d, J* = 8.4 Hz, 1H, Ar-H), 6.71 (*d, J* = 8.1 Hz, 2H, Ar-H dimethylamino) and 3.07 (*s*, 6H, N-$(CH_3)_2$). $^{13}$C NMR (600 MHz, DMSO- $d_6$): δ (ppm): 187.2, 163.3, 152.2, 144.2, 131.3, 130.9, 122.8, 116.8, 115.9, 112.3, 111.5 and 40.2.

#### 2.3.3. Synthesis of zinc (II) and indium (III) metallo-phthalocyanines (3 and 4), scheme 2

A procedure described in the literature with slight modifications [22] was used as follows: For phthalocyanine **3**, compound **2** (0.52 g, 1.31 mmol) and anhydrous zinc acetate (0.121 g, 0.66 mmol) were dissolved in pentanol (3 mL) under argon atmosphere followed by addition of a catalytic amount of DBU (three drops). For phthalocyanine **4**, compound **2** (0.5 g, 1.27 mmol) was dissolved in dry pentanol (3 mL) and anhydrous indium chloride (0.281 g, 1.27 mmol) was added followed by a few drops of DBU under argon atmosphere. The reaction mixtures for both **3** and **4** were heated at 160 °C while stirring for 24 h, cooled, and separately dissolved in ethanol with constant stirring for 1 h. Afterward, the mixtures were transferred into ice water and the resulting green solids were filtered and dried.

ZnPc (**3**): Yield: 42%. IR (UATR-TWO™) ν max/cm$^{-1}$: 2920 (Ar-H), 2903–2855 (Aliph C—H), 1716 (C = O), 1582–1462 (C = C, C = N), 1350 (C—C), 1220–1164 (*Asym.*, Ar-O-Ar), 1027 (*Sym.*, Ar-O-Ar), 816. $^1$H NMR (600 MHz, DMSO-$d_6$): δ (ppm): 8.29 (*d, J* = 8.7 Hz, 8H, Ar-H); 8.21 (*d, J* = 8.5 Hz, 2H, Ar-H Pc ring); 8.11 (*d, J* = 16.1 Hz, 4H, *trans*-H); 7.98 (*d, J* = 8.2 Hz, 2H, Ar-H Pc ring); 7.77 (*d, J* = 8.5 Hz, 2H, Ar-H Pc ring); 7.75 (*d, J* = 8.7 Hz, 8H, dimethylamino); 7.72 (*s*, 4H, Ar-H Pc ring); 7.47 (*d, J* = 16.0 Hz,4H, *trans*-H); 7.37 (*d, J* = 8.7 Hz, 8H, Ar-H); 7.27 (*d, J* = 8.7 Hz, 2H, Ar-H Pc ring); 6.83 (*d, J* = 8.7 Hz, 8H, Ar-H dimethylamino) and 3.09 (*s*, 24H, N-$(CH_3)_2$). Calcd. for $C_{100}H_{76}N_{12}O_8Zn$: C = 73.27, *H* = 4.67, *N* = 10.25, found: C = 73.23, *H* = 4.45, *N* = 9.95. MALDI TOF MS *m/z*: Calcd: 1639.13; Found: $[M + H]^+$= 1640.08.

InPc (**4**): Yield: 38%. IR (UATR-TWO™) ν max/cm$^{-1}$: 2919 (Ar-H), 2903–2855 (Aliph C—H), 1717 (C = O), 1582–1523 (C = C, C = N), 1462–1350 (C—C), 1220–1164 (*Asym.*, Ar-O-Ar), 1026 (*Sym.*, Ar-O-Ar), 817. $^1$H NMR (600 MHz, DMSO- $d_6$): δ (ppm): 8.31 (*d, J* = 8.2 Hz,8H, Ar-H); 8.20 (*d, J* = 8.1 Hz, 2H, Ar-H Pc ring); 8.10 (*d, J* = 16.2 Hz, 4H, *trans*-H); 8.01 (*d, J* = 8.0 Hz, 2H, Ar-H Pc ring); 7.77 (*d, J* = 8.2 Hz, 2H, Ar-H Pc ring); 7.75 (*d, J* = 8.5 Hz, 8H, Ar-H dimethylamino); 7.72 (*s*, 4H, Ar-H Pc ring); 7.49 (*d, J* = 16.4 Hz, 4H, *trans*-H); 7.37 (*d, J* = 8.1 Hz, 8H, Ar-H); 7.27 (*d, J* = 8.2 Hz, 2H, Ar-H Pc ring); 6.83 (*d, J* = 8.2 Hz, 8H, Ar-H dimethylamino) and 3.10 (*s*, 24H, N-$(CH_3)_2$). Calcd. for $C_{100}H_{76}ClInN_{12}O_8$: C = 69.67, *H* = 4.44, *N* = 9.71, found: C = 69.35, *H* = 4.89, *N* = 9.41. MALDI TOF MS *m/z*: Calcd: 1724.02; Found: $[M + H]^+$= 1725.21.

#### 2.3.4. Synthesis of the quaternized phthalocyanines (3a and 4a), scheme 2

A slightly modified protocol [29] was employed in this case, where phthalocyanines **3** (0.15 g, 0.091 mmol) or **4** (0.15 g, 0.087 mmol) were first dissolved in DMF (10 mL) under argon atmosphere, and an excess of iodomethane ($CH_3I$) was added, then the mixtures were stirred at reflux for 24 h. The reaction mixtures were then filtered and washed with acetone (3 times) by centrifugation and dried in vacuo to give quaternized complexes **3a** and **4a**. Dark green solids.

ZnPc (**3a**): Yield: 95%. IR (UATR-TWO™) ν max/cm$^{-1}$: 3043 (Ar-H), 2928–2855 (Aliph C—H), 1706 (C = O), 1656–1590 (C = C, C = N), 1464–1327 (C—C), 1220–1160 (*Asym.*, Ar-O-Ar), 1087 (*Sym.*, Ar-O-Ar), 828. $^1$H NMR (600 MHz, DMSO- $d_6$): δ (ppm): 8.25 (*d, J* = 8.2 Hz, 8H, Ar-H); 8.05 (*d, J* = 8.2 Hz, 8H, Ar-H); 7.95 (*d, J* = 8.7 Hz, 2H, Ar-H Pc ring); 7.93 (*d, J* = 15.7 Hz, 4H, *trans*-H); 7.72 (*d, J* = 8.7 Hz, 4H, Ar-H Pc ring); 7.68 (*d, J* = 8.3 Hz, 8H, Ar-H dimethylamino); 7.41 (*d*, 4H, *trans*-H); 7.32 (*d, J* = 8.5 Hz, 4H, Ar-H Pc ring); 7.23 (*d, J* = 8.7 Hz, 2H, Ar-H Pc ring); 6.83 (*d, J* = 8.2 Hz, 8H, Ar-H dimethylamino) and 3.03 (*s*, 36H, N-$(CH_3)_2$). Calcd. for $C_{104}H_{88}N_{12}O_8Zn$: C = 73.51, *H* = 5.22, *N* = 9.89, found: C = 73.24, *H* = 5.60, *N* = 9.84.

InPc (**4a**): Yield: 98%. IR (UATR-TWO™) ν max/cm$^{-1}$: 2923 (Ar-H), 2905–2856 (Aliph C—H), 1709 (C = O), 1657–1588 (C = C, C = N), 1461–1328 (C—C), 1212–1150 (*Asym.*, Ar-O-Ar), 1024 (Sym., Ar-O-Ar), 819. $^1$H NMR (600 MHz, DMSO- $d_6$): δ (ppm): 8.24 (*d, J* = 8.7 Hz, 8H, Ar-H); 8.05 (*d, J* = 8.7 Hz, 8H, Ar-H); 7.95 (*d, J* = 8.2 Hz, 2H, Ar-H Pc ring); 7.93 (*d, J* = 16.0 Hz,4H, *trans*-H); 7.72 (*d, J* = 8.1 Hz, 4H, Ar-H Pc ring); 7.68 (*d, J* = 8.5 Hz, 8H, Ar-H dimethylamino); 7.41 (*d, J* = 16.2 Hz, 4H, *trans*-H); 7.32 (*d, J* = 8.9 Hz, 4H, Ar-H Pc ring); 7.23 (*d, J* = 8.7 Hz, 2H, Ar-H Pc ring); 6.83 (*d, J* = 8.6 Hz, 8H, Ar-H dimethylamino) and 3.04 (*s*, 36H, N-$(CH_3)_2$). Calcd. for $C_{104}H_{88}ClInN_{12}O_8$: C = 70.01, *H* = 4.97, *N* = 9.42, found: C = 70.47, *H* = 4.57, *N* = 9.74.

### 2.4. Photophysical and photochemical studies

Details are provided in the Supporting Information. Briefly, fluorescence quantum yield ($\Phi_F$) and singlet oxygen quantum yield ($\Phi_\Delta$) were determined using comparative methods using unsubstituted ZnPc dissolved in DMSO as a standard ($\Phi_F$ = 0.2 [30], $\Phi_\Delta$ = 0.67 [31]). Singlet oxygen generation efficacy was also tested in an aqueous solution using AlPcSmix in 1% DMSO aqueous media ($\Phi_\Delta$ = 0.42 [31]) as the standard. Diphenylisobenzofuran (DPBF) and anthracene-9, 10-bis-methylmalonate (ADMA) were used as singlet oxygen chemical quenchers in DMSO and aqueous media respectively, and their degradation was monitored at 417 nm and 378 nm, respectively.

### 2.5. PACT/PDT studies

Further details for these studies may be found in the supporting information

For PACT studies, 1% DMSO in PBS was used to prepare concentrations of 0.63, 1.25, 2.50, 5, 10, and 20 μM for planktonic cells. For biofilms, the concentrations of the photosensitizers used were 25, 50, and 100 μM. 1% DMSO in PBS solutions containing only bacteria were considered as control groups. Irradiation was for 120 min at 30 min intervals using a Modulight laser lamp (670 nm, 524 mW/cm$^{2,}$ and dose: 943 J/cm$^2$), for both biofilm and planktonic cultures of pathogenic bacteria. For PDT studies the concentrations of the photosensitizers ranged from 0.8 to 50 μM and irradiation was 15 min using a Modulight laser lamp (670 nm, 524 mW/cm$^2$).

## 3. Results and discussion

### 3.1. Synthesis and characterization

Large substituents on peripheral or non-peripheral positions of phthalocyanines and the presence of heavy central metals in their core can result in reduced aggregation and improved solubility [32,33]. The synthesis of the bulky chalcone derivative (**1**) used in the present work is depicted in Scheme 1. The dimethylamino chalcone (**1**) was synthesized quantitatively by a Claisen-Schmidt condensation of 4-hydroxyacetophenone and 4-dimethylaminocarbaxaldehyde using KOH as the base. Then the new chalcone-derived phthalonitrile (**2**, Scheme 1) was obtained through a classical nucleophilic substitution reaction between chalcone (**1**) and 4-nitrophthalonitrile in DMF using $K_2CO_3$ as the base. The molecular structures of **1** and **2** were all confirmed based on NMR, **Fig. S1–4** in the Supporting Information (SI).

It is illustrated in $^1$H NMR (**Fig. S1,** for **1**) that the two doublet peaks resonating at 7.67 and 6.78 are attributed to *trans* protons (CH═CH) and a broad singlet peak at 9.66 corresponds to the OH proton while in $^{13}$C NMR (**Fig. S2**), $\delta_C$ 136.9 and 121.3 correspond to the alpha, betaunsaturated carbons (CH═CH) and 190.5 to the carbonyl group (C = O). The [1]H and [13]C NMR data (**Fig. S3** and **S4**) of compound **2** agreed with the proposed structure, exhibiting the disappearance of characteristic peaks such as the -OH proton peak and the appearance of -CN carbon peaks at 115.9 in the [13]C NMR spectrum as shown in **Fig. S4** in SI. Similar NMR results have been reported elsewhere regarding the coupling constant [22,28].

Through cyclotetramerization reaction of the phthalonitrile **2** using zinc acetate dihydrate and indium chloride salts respectively, and DBU as the catalyst at high temperature, phthalocyanines **3** and **4** were obtained, Scheme 2. Then their quaternized analogs **3a** and **4a** were prepared following *the N*-methylation reaction of both **3** and **4** Pcs using iodomethane as a methylating agent in DMF at reflux temperature.

The novel phthalocyanines bearing chalcone group were all characterized by FT-IR, UV–Vis, mass spectrometry, [1]H NMR spectroscopy performed in deuterated DMSO as well as EDX (see **Figs. S5-S9** in the SI) and CHN elemental analysis.

[1]H NMR spectra of the phthalocyanines exhibit peaks with slight chemical shift differences as seen in the SI. In these spectra, integrals of the aromatic region together with the aliphatic area (3.09–8.31 ppm, 76 protons in total) for complexes **3** and **4** (**Fig. S7** using complex **3** as an example) compared to the (3.03–8.25 ppm, 88 protons in total) for complexes **3a** and **4a** (**Fig. S8** using **4a** as an example) were consistent with the proposed structures.

In addition, mass spectrometry was also used for the structure elucidation of the synthesized Pcs. The acquired spectra show that the desired compounds were obtained as expected whereas the molecular ion peaks were identified at $[M + H]^+ = 1640.08$ $m/z$ for complex **3** and $[M + H]^+ = 1725.21$ $m/z$ for complex **4**, **Figs. S5** and **S6**. The quaternised complexes **3a** and **4a** did not ionize with α-cyano hydroxycinnamic acid matrix, hence no data were obtained. The EDX analysis was also used to determine the elemental composition of the complexes. As it is shown in **Fig. S9** in the SI, elements such as C, N, Cl, Zn, and In were present in the spectra of the Pc derivatives. We note that sulfur peak comes from DMSO, used for dissolving the Pcs for coating the grit and drying for EDX spectra. Experimental elemental analysis (CHN) is in agreement with theoretical values.

Fig. 1 clearly shows the FT-IR spectra of all the desired products. The broad band observed at 3094 $cm^{-1}$ in the spectrum for compound **1** is assigned to O—H stretching vibration. The absence of this band (at 3094 $cm^{-1}$) in the spectrum of compound **2** in addition to the presence of the C☰N characteristic band at 2225 $cm^{-1}$ gives a specific indication of the successful synthesis of chalcone-derived phthalonitrile (**2**). Stretches observed in the 3043–2710 $cm^{-1}$ regions are attributed to the aromatic and aliphatic C—H bonds and those around 1657–1462 $cm^{-1}$ are due to C = C and C = N vibrations. The stretching vibrations due to the C = O bond in compounds **1** and **2** can be attributed to the bands observed at 1663 and 1667 $cm^{-1}$ respectively. After the cyclotetramerization of phthalonitrile derivative **2**, the C = O band shifted to about 1716 and 1717 $cm^{-1}$ (for **3** and **4**, respectively) and 1706 and 1709 $cm^{-1}$ (for **3a** and **4a**, respectively). The disappearance of the C☰N band was also observed clearly for all the Pcs. The disappearance of this band can be considered as proof of cyclotetramerization of the phthalocyanine complexes. The bands in the FT-IR spectra of quaternized derivatives **3a** and **4a** show very similar peaks to their non-quaternized counterparts.

The UV–Vis absorption spectra for **3, 3a, 4,** and **4a** recorded in DMSO are shown in Fig. 2. Generally, the Q-band (the most important band for excitation in PACT/PDT) is attributed to the π→π* transition from the highest occupied molecular orbital (HOMO) to the lowest unoccupied molecular orbital (LUMO) of the Pc macrocycle whereas the B-band result from deeper π levels to the LUMO transitions [34]. The electronic absorption spectra (Fig. 2) of the synthesized compounds are typical of non-aggregated Pcs in DMSO as they exhibit intense and sharp Q-bands between 680 and 689 nm (Table 1). Compared with ZnPc derivatives, the InPc counterparts show red-shifts (5 to 6 nm) in $\lambda_{max}$ of respective Q-bands as can be observed in Table 1. The red-shifts are due

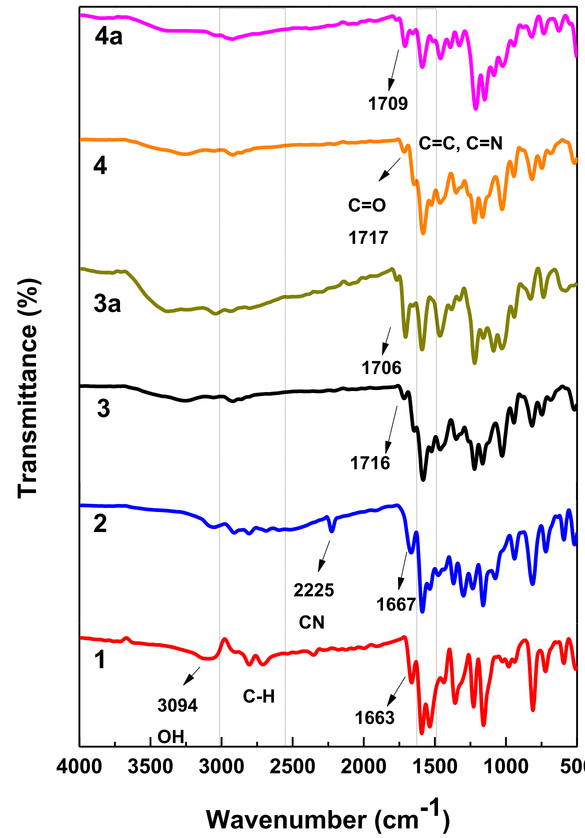


**Fig. 1.** FT-IR spectra of the synthesized compounds.

to the non-planar effect of the In(III) ion and its bigger atomic radius compared to Zn(II) ions [35,36]. Interestingly, a further red-shift was observed in the absorption maxima of the Q-bands of the quaternized **3a** and **4a**.

When the spectra were recorded in aqueous media (1% DMSO in water v/v), aggregation was observed as judged by the presence of two non-vibrational peaks in the Q band region [35], Figs. 2**A, B** (using **3a** and **4a** as examples) and Table 1. Aggregation (the so-called H aggregates) in phthalocyanines is judged by a broad or split Q band with the high energy band being due to the aggregate and the low energy band to the monomer. The bands due to the monomer are observed at 688, 691 nm (for **3, 3a**) and 690, 695 nm (for **4, 4a**), and the aggregate peaks at 649, 647 nm (for **3, 3a**) and 651 nm (for both **4, 4a**).

The synthesized chalcone (**1**) shows an absorption band at 416 nm (Fig. 3) which is due to π-π* electronic transitions. *Trans*-Chalcones are usually reported to show two absorption bands belonging to the *n*-π* (intense absorption band around 220–270 nm) and π-π* (weaker absorption band above 350 nm) transitions [37].

### 3.2. Photophysicochemical properties

#### 3.2.1. Emission and energy transfer study

Emission spectra of all the phthalocyanines complexes were recorded in DMSO at $\lambda_{exc}$ 400 nm and 606 nm to excite chalcone and Pc core, respectively. Upon excitation at 606 nm in DMSO, the four Pcs showed fluorescence emission with stokes shift less than 10 nm when compared to the corresponding excitation spectra. The emission spectra of the cationic Pcs are illustrated in Fig. 4 as examples and the corresponding data are summarized in Table 1. The excitation and absorption spectra were similar (slight differences in peak maxima are due to different equipment used) and both were mirror images of the emission spectra for all studied phthalocyanines**, Fig. S10 in the SI**. This indicates that the absorbing and emitting molecules are the same [38,39].

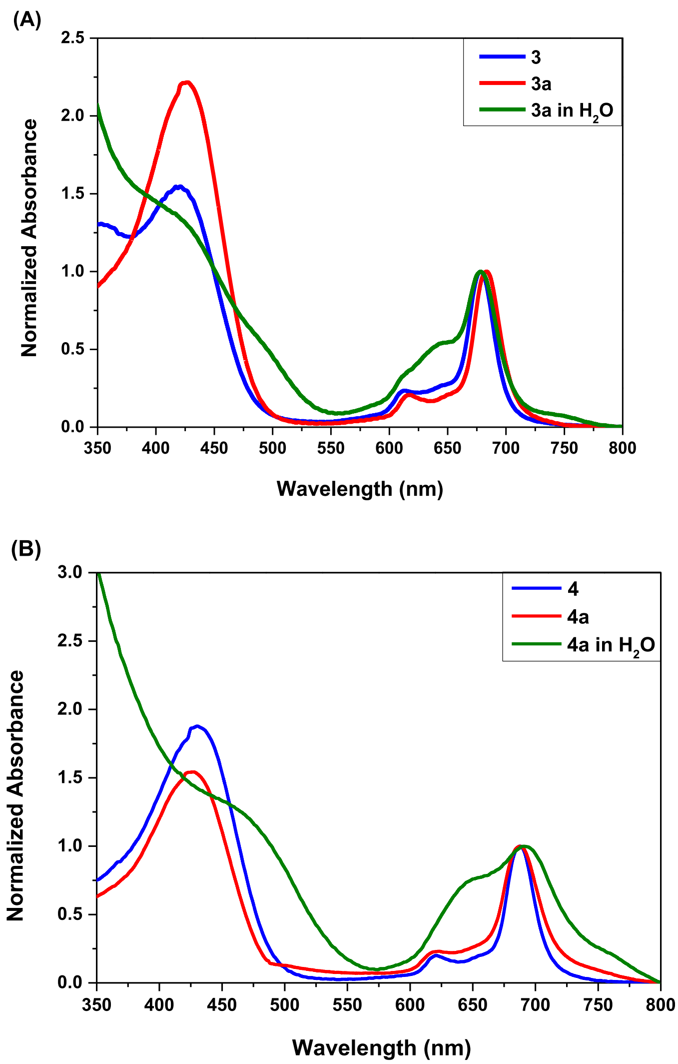


**Fig. 2.** Normalized electronic absorption spectra of phthalocyanine complexes (**A**) **3**, **3a** in DMSO and **3a** in water (1% DMSO); (**B**) **4**, **4a** in DMSO and **4a** in water (1% DMSO).

### 3.2.2. *Fluorescence quantum yield ($\Phi_F$) and fluorescence lifetime ($\tau_F$)*

The fluorescence quantum yield ($\Phi_F$) determines the efficiency of the fluorescence process, a process in which a photosensitizer in the first singlet excited state degenerates to the ground state emitting its energy in the form of fluorescence.

The $\Phi_F$ is the ratio of the number of photons emitted to the number of photons absorbed by a photosensitizer. In the present report, the $\Phi_F$ values were obtained in DMSO following comparative methods reported in the literature [30] (details may be found in the supporting information). The $\Phi_F$ values of the studied phthalocyanines are reported in Table 1. At $\lambda_{exc}$ = 606 nm, the complexes had fluorescence quantum yields ($\Phi_F$) ranging from < 0.01 to 0.061, relative to ZnPc standard ($\Phi_F$ = 0.20). The low $\Phi_F$ values could be due to the Pc core self-quenching effect, but mostly from nitrogen atom on the substituent causing the intramolecular charge transfer (ICT) and the presence of large central metal atoms [30–41] which are known to enhance the intersystem crossing process to the triplet state, thus limiting the fluorescence process to take place [39] even though chalcone compounds are fluorescent by nature.

The $\Phi_F$ values for InPcs were lower than those of ZnPcs due to the heavier central atom of the former effect which is known to enhance the intersystem crossing to the triplet state, thus reducing fluorescence [38].

However, when exciting at 400 nm where chalcone absorbs, the complexes showed two very weak emission peaks at 525 for the chalcone and around 700 nm for the Pc core (Fig. 5) with $\Phi_F$ values ranging from as 0.008–0.014 as illustrated in Table 1. The decrease in the emission intensity of compound **1** when combined with Pc could be due to the Förster resonance energy transfer (FRET) *via* covalent bond from the donor chalcone moieties to the acceptor Pc core and/or numerous other factors which deactivate the excited states [42]. The FRET efficiency (*Eff*) was determined using equation 1.

$$Eff = 1 - \frac{\Phi_{F\ (Pcs)}}{\Phi_{F\ (chalcone)}} \tag{1}$$

where $\Phi_F$ (Pcs) and $\Phi_F$ (chalcone) are the fluorescence quantum yields of the acceptor (chalcone-substituted Pcs) and the donor alone (chalcone) excited at 400 nm, respectively.

As depicted in Table 1, the *Eff* values are almost the same for all the

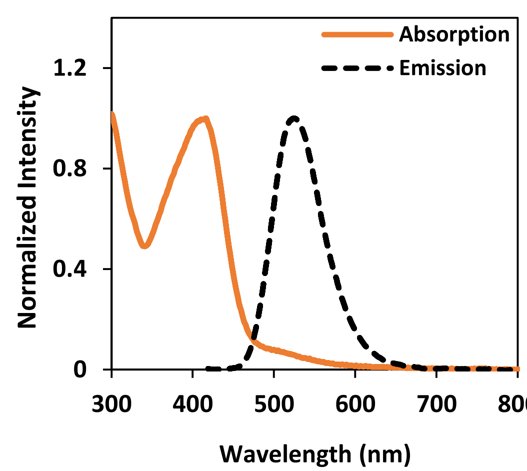


**Fig. 3.** Normalized absorption and emission spectra of chalcone **1** in DMSO.

**Table 1**
Photophysicochemical parameters of the chalcone, non-quaternized Pcs, and quaternized Pcs in DMSO.

| Sample | Abs.[a,b](nm) | Exc.[a](nm) | Em.[a] | $\Phi_F$ [c] | Eff (%) | $\tau_F$(ns) | $\Phi_\Delta$[a] |
|---|---|---|---|---|---|---|---|
| **1** | 416 | – | 525 [c] | 0.18 | – | – | – |
| **3** | 680<br>(688, 649) | 682 | 689 | 0.061<br>(0.014) | 92 | 2.88 | 0.43<br>(0.09) |
| **4** | 686<br>(690, 651) | 686 | 691 | <0.01<br>(0.011) | 94 | 2.46 | 0.50<br>(0.11) |
| **3a** | 684<br>(691, 647) | 682 | 689 | 0.053<br>(0.012) | 93 | 2.88 | 0.48<br>(0.20) |
| **4a** | 689<br>(695,651) | 686 | 691 | 0.019<br>(0.008) | 95 | 2.36 | 0.57<br>(0.24) |

[a] Abs = absorbance, Exc = excitation, Em = Emission.
[b] Values in brackets are in water (containing 1% DMSO) used for cell studies. [c] values in brackets are for excitation where chalcone absorbs ($\lambda_{exc}$ = 400 nm), the values not in brackets are for exciting the Pc ring at 606 nm.

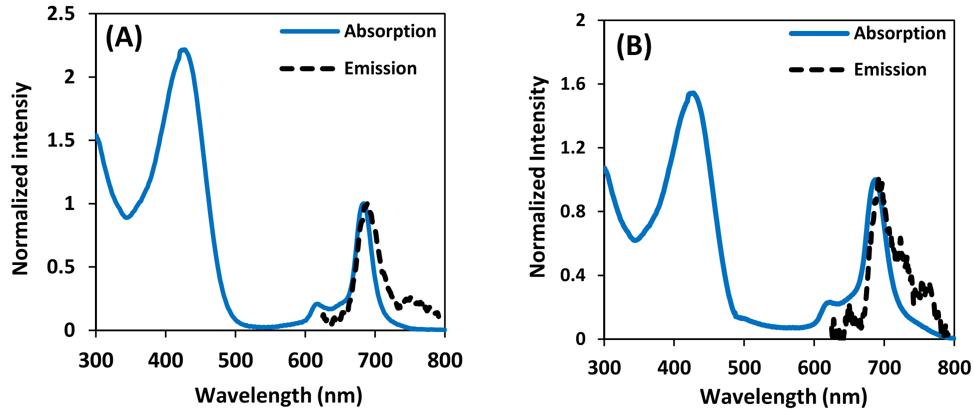


**Fig. 4.** Normalized absorption and emission spectra of (**A**) **3a** and (**B**) **4a** in DMSO with excitation at 606 nm (from Pc).

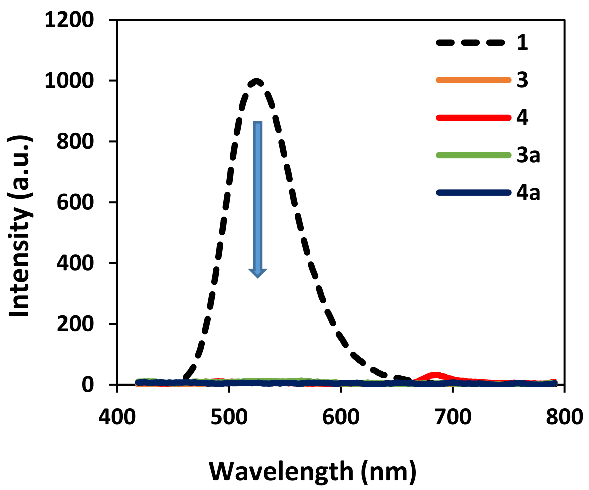


**Fig. 5.** Emission spectra of **1** and all the Pc complexes in DMSO with excitation at 400 nm.

studied compounds; 92, 94, 93, and 95% for **3, 4, 3a,** and **4a** respectively. This implies that there is a similar spectral overlap and shows that there are efficient energy transfer processes for these Pc systems.

Another important factor considered in this work is the fluorescence lifetime ($\tau_F$). It refers to the average time a molecule spends in its first singlet excited state before it undergoes the fluorescence process [30, 41]. The $\tau_F$ values of studied complexes were obtained in DMSO using the time correlation single photon counting (TCSPC) method and the fluorescence decay curve shown in Fig. 6 (as an example) and **Fig. S11** in the supporting information. Mono exponential decay curves were obtained with lifetimes of 2.88 ns for **3**, 2.46 ns for **4**, 2.88 ns for **3a,** and 2.36 ns for **4a**. These values are typical for MPcs [36]. $\tau_F$ values are long where the $\Phi_F$ values are high as expected.

### 3.2.3. *Singlet oxygen quantum yield ($\Phi_\Delta$)*

As stated above, ROS are responsible agents for the target bacteria cells' damage. Amongst ROS, singlet oxygen ($^1O_2$) has been demonstrated to be the main cytotoxic component. Therefore, it is crucial to evaluate the $^1O_2$ generation abilities of photosensitizers to determine how efficient their photosensitizing effect is.

As can be seen in Figs. 7 **(A, B)** and **Fig. S12** in the SI, the generated

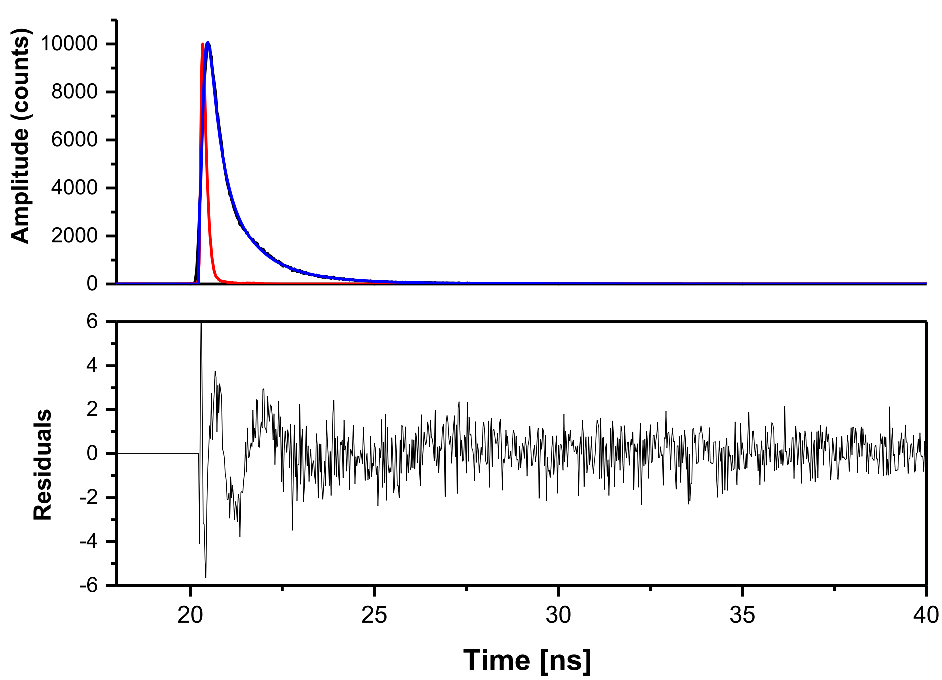


**Fig. 6.** TCSPC fluorescence decay curve of **4a** (as an example).

singlet oxygen by the phthalocyanines react with chemical quenchers thus causing a decrease in the absorbance of the latter. Hence, we monitored these decreases at 417 and 378 nm for DPBF and ADMA respectively, using a UV–Vis spectrophotometer. No change in absorption intensities of the Pcs Q-bands throughout the irradiation time confirms the stability of the molecules in the currently applied experimental conditions.

The $\Phi_\Delta$ values were ranging between 0.43 and 0.57 with the highest values being for the quaternized derivatives in DMSO as seen in Table 1. The reason is that the photoinduced electron transfer (PET) process between the core and chalcone-substituent of Pcs cannot be detected in **3a** and **4a**, since the lone pair electrons on nitrogen atoms are bonded to methyl groups in the positively charged entities [43]. In a 1% DMSO medium, the complexes have lower $\Phi_\Delta$ values (Table 1) due to the quenching of singlet oxygen by water [30]. With such photosensitizing properties, the newly prepared chalcone-derived Pcs can be exploited for PACT/PDT applications.

### 3.3. PACT studies

#### 3.3.1. Planktonic cultures of pathogenic bacteria

The rising rates of antibiotic-resistant *E. coli* and *S. aureus* infections have become a major concern for health systems [44,45]. Therefore, in the present work, the photodynamic antibacterial activities of the newly prepared positively charged Pcs as well as their non-charged derivatives were investigated.

From the optimization experiments, it is seen in Figs. 8**A** and 9**A** that concentrations of 10 and 1.25 μM were best for the non-quaternized and quaternized Pcs, respectively. The optimal concentrations are the lowest values at which compounds can still exhibit antimicrobial potency by inhibiting more than 50% of the bacteria.

Figs. 8 and 9 (**B, C**) show the Log CFU/mL, Figs. 8 and 9(**D**) show percentage bacteria survival plots respectively, in the absence and presence of light and Figs. 8**E** and 9**E** show examples of agar plates photographs. Noticeably, all the studied compounds are basically non-cytotoxic in the dark, except for the quaternized complexes **3a** and **4a** that exhibited some dark cytotoxicity with log reductions of 1.29 and 1.41 respectively on *S. aureus* while on *E. coli* these values were of 1.20 and 1.24 Log reduction. Similarly, other reports have shown that the incubation of *E. coli* with cationic phthalocyanine in the dark caused alterations of the outer membrane permeability and increased the cell uptake [46].

According to our results, *S. aureus* strain was found to be more susceptible than *E. coli* strain to the PACT considering the $Log_{10}$ CFUs (Table 2). In agreement with our findings, it has been reported that PACT is more effective on Gram-positive bacteria (i.e., *S. aureus*) as compared to Gram-negative bacteria (i.e., *E. coli*) due to the differences in their cell wall structures [47]. This was confirmed as complexes **3** and **4** exhibited significant reduction on the bacteria strains with 3.23 $Log_{10}$ reduction (0.05% survival cells) and 3.69 $Log_{10}$ reduction (0.02% survival cells), respectively on *S. aureus*. When tested on *E. coli*, values of 2.84 and 2.99 $Log_{10}$ reductions were respectively obtained. Literature has reported that the double-layered cell membrane of Gram-negative bacteria such as *E. coli* can be a barrier to neutral or negatively charged photosensitizers to get inside the cell [48]. Therefore, the photodynamic killing of Gram-positive bacteria such as *S. aureus* can be much easier to accomplish than that of Gram-negative bacteria such as *E. coli*.

Upon 30 min of irradiation with light, phthalocyanines **3a** and **4a** present a much higher photocytotoxicity for *S. aureus* with 10.48 $Log_{10}$ reduction with no viable cells whereas a 9.30 $Log_{10}$ was obtained for *E. coli*. From the results in Table 2, we can speculate that the positive charges of phthalocyanines **3a** and **4a** easily bind to the surface of bacterial cells by strong electrostatic interactions which may cause the breakage of cytoderm, thereby easing their penetration into the cytoplasm, thus enhancing cellular uptake. Positively charged groups present in photosensitizer may play an important role in modulating the efficacy of the photoinactivation process against microbial cells [49]. The PACT activities obtained perfectly agrees with the singlet oxygen production ability of the novel photosensitizers in this work.

#### 3.3.2. Biofilms

In our work, to fill data gaps, we examined the antimicrobial activity of the novel Pcs against two of the most pertinent bacteria, we selected the major biofilm producers, *S. aureus* and *E. coli*, well known to affect the population's wellbeing. Following the impressive results of the photodynamic activities on their planktonic counterparts, we proceeded to analyze the ability of the studied Pcs to eradicate the biofilm previously formed by these bacteria.

In this case, the strains were treated with different Pcs, in concentrations of 25, 50, and 100 μM. Their activities were compared to the control groups as described in the experimental part of this work (presented in Supporting Information). From the listed data in Table 3, Pcs **3a** (2.1 and 4.5% cell survival) and **4a** (1.2 and 2.3% cell survival), respectively for *S. aureus* and *E. coli,* significantly inhibit both biofilm strains at 100 μM after only 30 min exposition to red light (Fig. 10**B** and 11**B**). The percentage survival was found to be 44 (8.4) and 48 (10)% on *S. aureus* and *E. coli*, respectively for **3** (**4** in brackets) at the highest

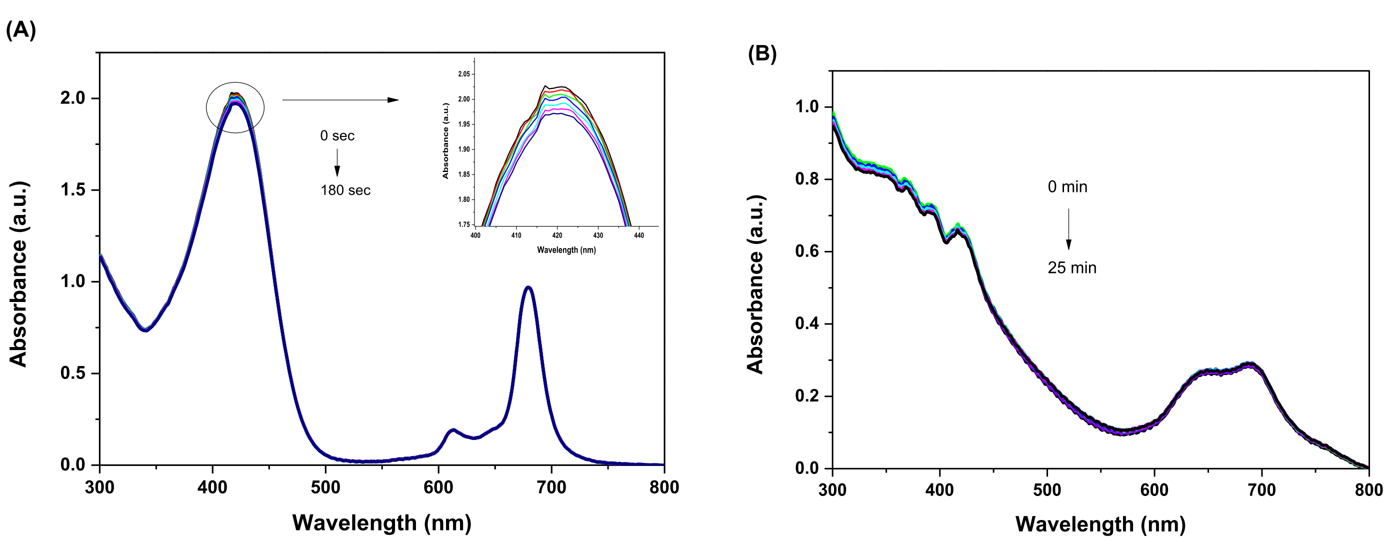


**Fig. 7.** A typical spectrum for the determination of singlet oxygen quantum yield of (**A**) **3** in DMSO using DPBF and (**B**) **3a** in water (1% DMSO) using ADMA.

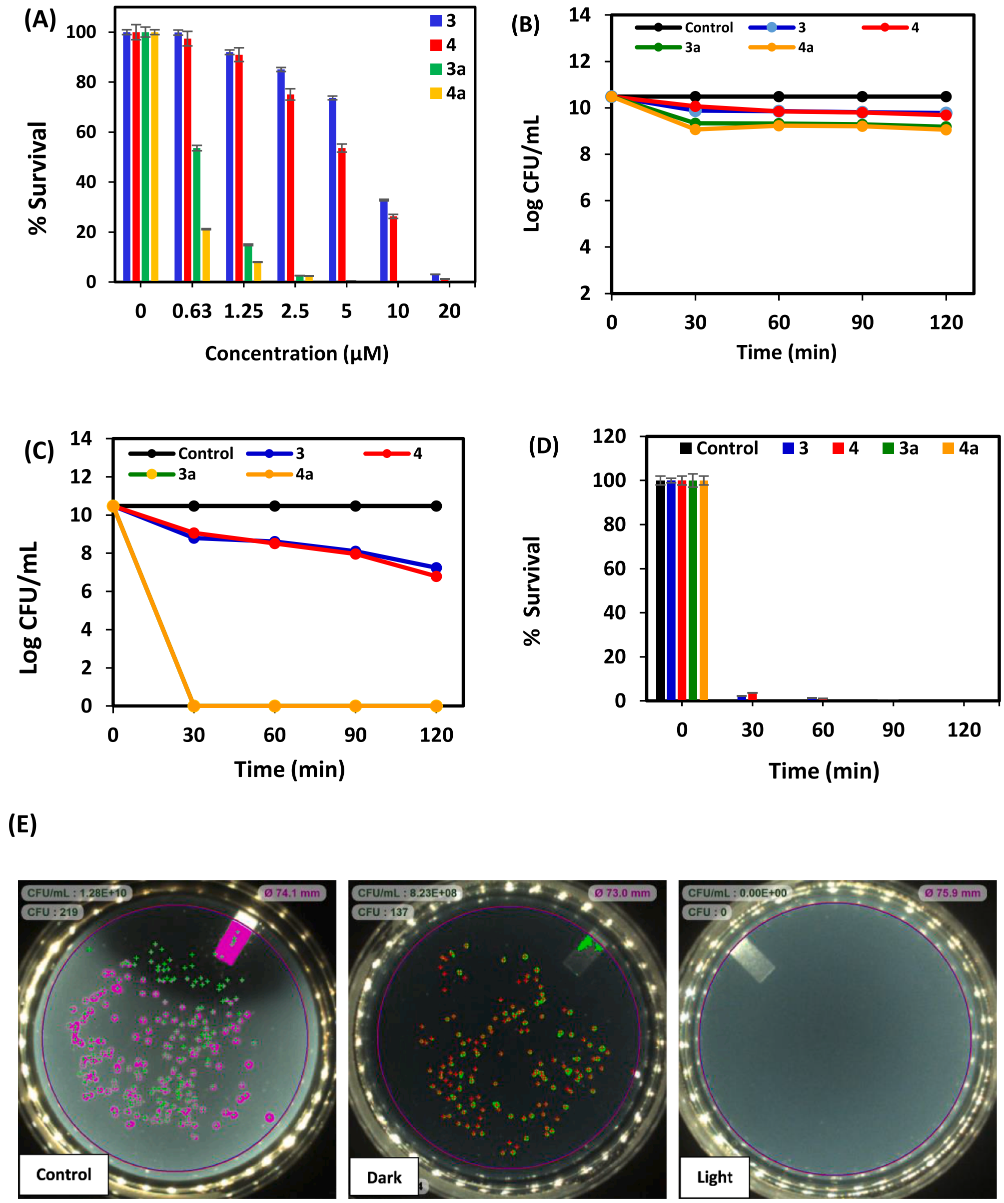


**Fig. 8.** (**A**) % Cell survival of complexes at different concentrations upon 30 min irradiation. $Log_{10}$ CFU/mL graphs for (**B**) Dark toxicity, (**C**) PACT studies on *S. aureus,* (**D**)% survival vs time graphs for planktonic cells with irradiation at 670 nm. The concentration of the drugs = 10 μM for non-quaternized and 1.25 μM for the cationic complexes. Data represent the mean ± SD (triplicate). (**E**) Agar plate photographs of **4a** (as an example) on *S. aureus*.

concentration of 100 μM. As mentioned before, in this case, the low activity obtained for complex **3** could be due to the absence of positive charges and bit of aggregation. Notably, recent work by us has demonstrated the photocytotoxic effects of different positively charged Pcs on both biofilm strains [22]. The preferential affinity of **3a** and **4a** to the studied strains should be related to their positive charges. This may be the main reason for the more efficient uptake by cells living in the biofilm forms.

It is important to also note that the group of samples kept in the dark with the same concentrations of photosensitizers did not demonstrate dark cytotoxicity effects on the strains as it can be observed in Figs. 10**A** and 11**A**.

### 3.4. Cancer cell studies

#### 3.4.1. Cellular uptake

The in vitro cellular uptake was investigated by measuring the absorbance of internalized complexes following 24 h drug incubation with MCF-7 cancer cells. Fig. 12 shows that quaternized complexes (**3a** and **4a**) have better cellular uptake than non-quaternized counterparts (**3** and **4**). Positively charged photosensitizers are known to internalize into the cell more favorably than anionic or neutral species due to negatively charged cell surface [50]. Cationic photosensitizers bind electrostatically to anionic regions of cell surface and facilitate the transport of cationic photosensitizers into the cells thereby increasing the PDT efficacy [50]. In comparison to the zinc analogs, the indium Pc presented higher internalization in the cells, the reason could be that the latter metal ion possesses a higher affinity to MCF-7 cancer cells.

#### 3.4.2. Photocytotoxicity studies in MCF-7 cells

To assess the PDT effect of the Pcs (**3, 4, 3a,** and **4a**) on MCF-7 cancer cells, their photocytotoxicities were quantitatively determined using a conventional MTT (methylthiazolyl-diphenyltetrazolium bromide) cell viability assay [51]. Firstly, the cancer cells were incubated with different drug concentrations ranging between 0.8–50 μM for 24 h.

The assay was carried out on the cells that were not irradiated to

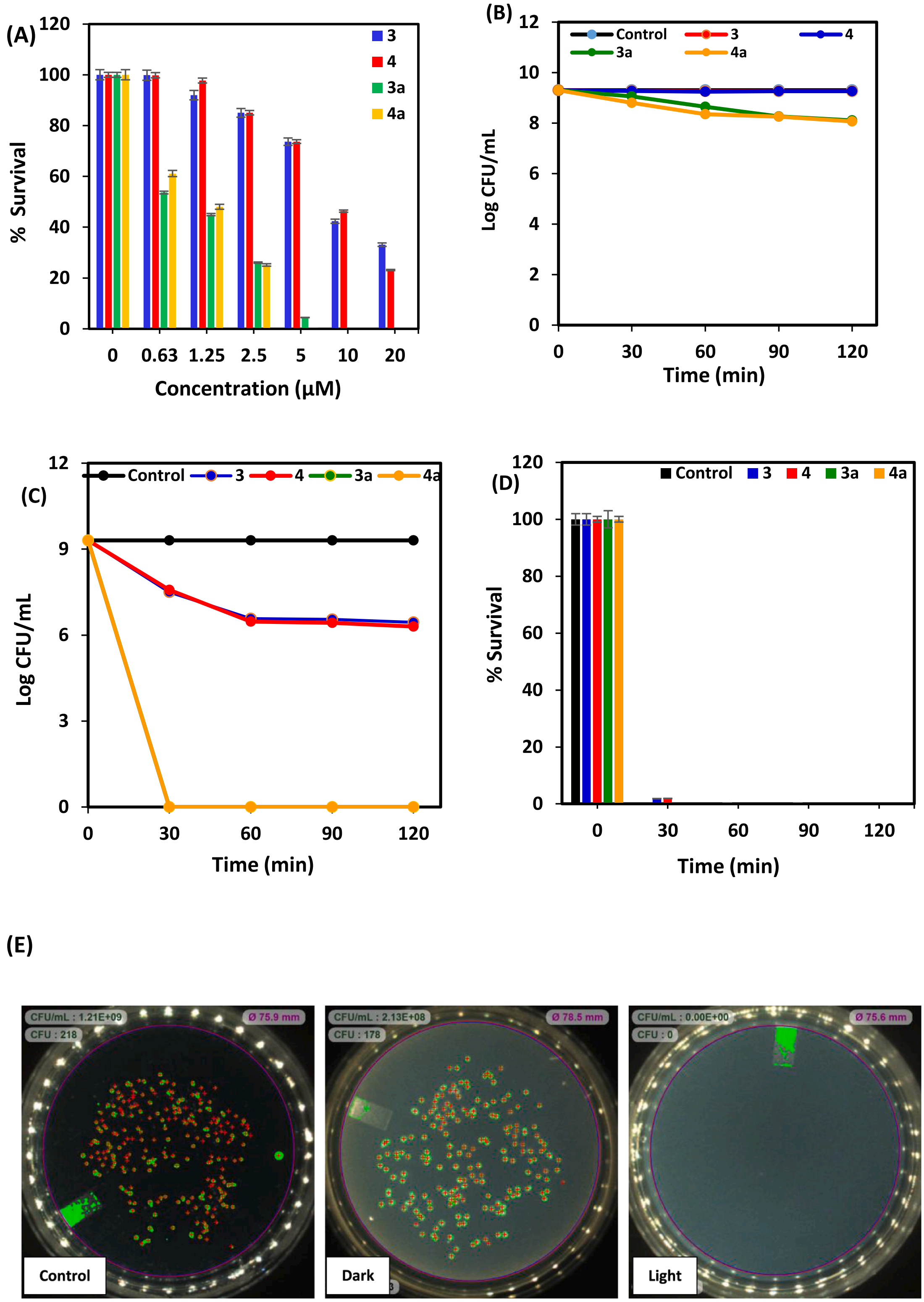


**Fig. 9.** (**A**) % Cell survival of complexes at different concentrations upon 30 min irradiation. $Log_{10}$ CFU/mL graphs for (**B**) Dark toxicity, (**C**) PACT studies on *E. coli,* and (**D**)% survival vs time graphs for planktonic cells with irradiation at 670 nm. The concentration of the drugs = 10 μM for non quaternized and 1.25 μM for the cationic complexes. Data represent the mean ± SD (triplicate). (**E**) Agar plate photographs of **4a** (as an example) on *E. coli.*

evaluate their dark toxicity and the results show that the compounds exhibit relatively insignificant dark toxicity with above 75% cell viability at 50 μM) (Fig. 13**A**).

However, the cell viability was significantly lower after exposure to light, indicating that the observed dramatic cytotoxicity activity resulted from irradiation at the tested concentrations. The cytotoxicity damage to the target cells was quantitated using $IC_{50}$ (50% inhibitory concentration calculated using GraphPad Prism software) values and the results are summarized in Table 4.

Upon 15 min irradiation at 670 nm with 524 mW/cm$^2$, complexes **3a**

**Table 2**
Log reduction and% survival data of 10 μM for non-quaternized and 1.25 μM for quaternized samples in 1% DMSO after irradiation.

| Sample | *S. aureus* | | | *E. coli* | | |
|---|---|---|---|---|---|---|
| | Log reduction | % Survival | Time of irradiation (min) | Log reduction | %Survival | Time of irradiation (min) |
| **3** | 3.23 | 0.05 | 120 | 2.84 | 0.14 | 120 |
| **4** | 3.69 | 0.02 | 120 | 2.99 | 0.10 | 120 |
| **3a** | 10.48 | 0 | 30 | 9.30 | 0 | 30 |
| **4a** | 10.48 | 0 | 30 | 9.30 | 0 | 30 |

**Table 3**
The% survival data of samples in 1% DMSO after 30 min irradiation on *S. aureus* and *E. coli* biofilms.

| Sample | % Survival | | | | | |
|---|---|---|---|---|---|---|
| | *S. aureus* | | | *E. coli* | | |
| | 25 μM | 50μM | 100μM | 25μM | 50 μM | 100 μM |
| 3 | 87 | 52 | 44 | 98 | 63 | 48 |
| 4 | 65 | 39 | 8.4 | 84 | 45 | 10 |
| 3a | 10 | 8.4 | 2.1 | 26 | 14 | 4.5 |
| 4a | 6.5 | 5.2 | 1.2 | 15 | 7.6 | 2.3 |

and **4a** exhibited $IC_{50}$ values of 17.9 and 7.4 μM respectively, and these values were relatively lower than those observed for **3** and **4** (20.4 and 12.1 μM, respectively. These results could be attributed to the higher cellular uptake observed for the quaternized complexes above. Also, previous studies have proven that PDT efficacy relies on the photosensitizer's ability to generate cytotoxic ROS in the target cells [52]. This observation indicates that **3a** and **4a** are suitable for PDT due to their ROS-generating ability in the cells, their affinity to the target cells, and efficient cellular uptake. The indium complexes (**4** and **4a**) showed higher PDT activity (Fig. 13**B**) with only 5.6 and 3.3% cell viability respectively at 50 μM compared to the corresponding zinc complexes **3** and **3a** which showed cell viability of 13.6 and 8.6%, respectively at the

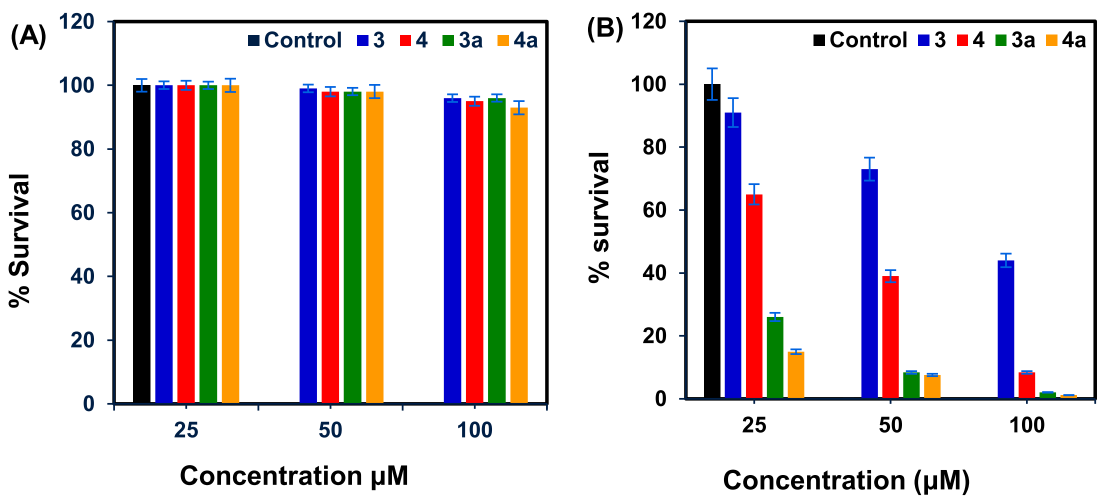


**Fig. 10.** Cell survival graphs for (**A**) Dark toxicity and (**B**) PACT studies for *S. aureus* biofilms with irradiation at 670 nm for 30 min. The concentration of the drugs = 25, 50 and 100 μM. Data represent the mean ± SD (triplicate).

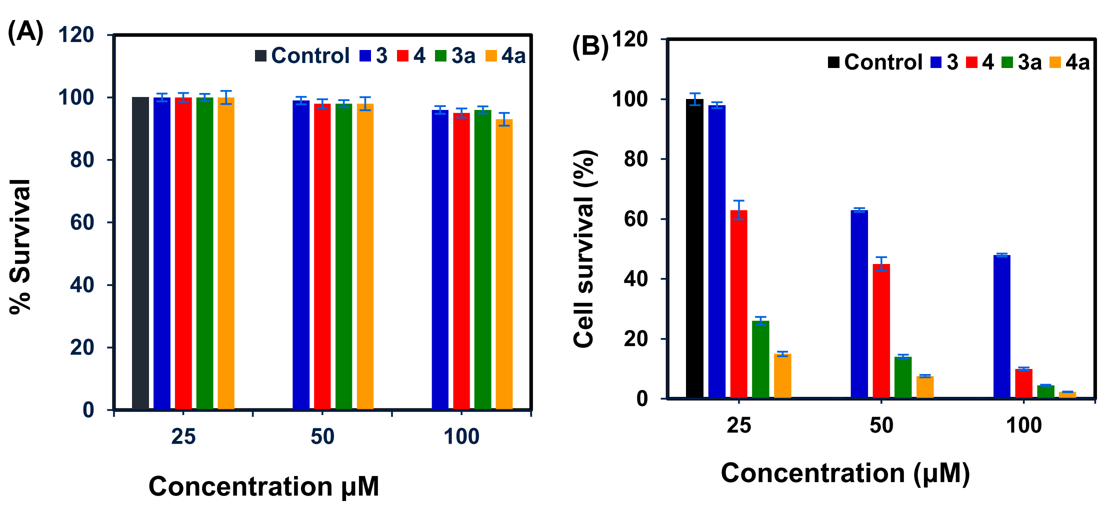


**Fig. 11.** Cell survival graphs for (**A**) Dark toxicity and (**B**) PACT studies for *E. coli* biofilms with irradiation at 670 nm for 30 min. The concentration of the drugs = 25, 50 and 100 μM. Data represent the mean ± SD (triplicate).

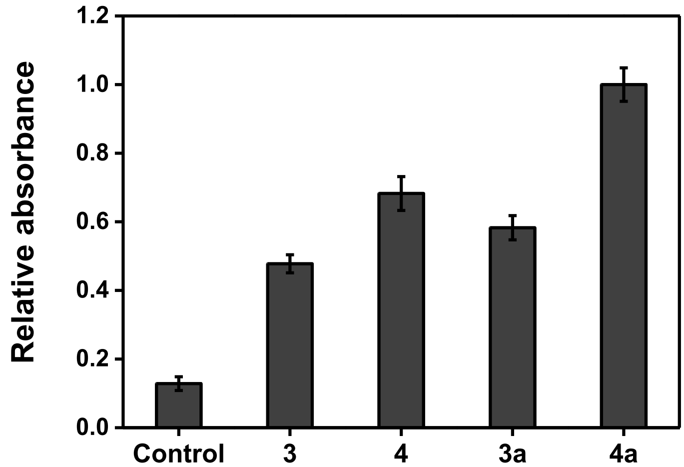


**Fig. 12.** Relative cellular uptake plot for **3**, **4**, **3a**, and **4a** by measuring the absorbance 670 nm with a multi-plate reader.

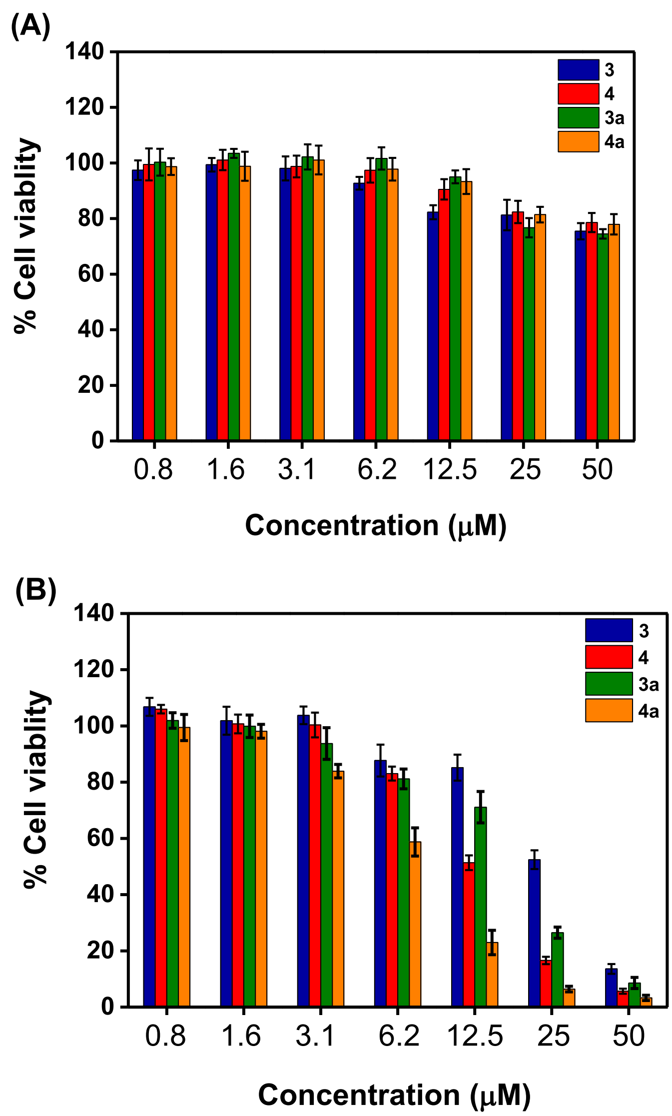


**Fig. 13.** Cytotoxicity of **3**, **4**, **3a**, and **4a** in MCF-7 cells after 24 h incubation in the (**A**) studies in the dark and (**B**) photo-irradiation (15 min) with a 670 nm light as determined by MTT assay.

**Table 4**
Phototoxicity (at 670 nm with 524 mW/cm$^2$ for 15 min) of the studied complexes against MCF-7 cancer cells.

| Sample | $IC_{50}$(μM) | % Cell viability at 50 μM |
|---|---|---|
| **3** | 20.4 ± 1.1 | 13.6 ± 1.7 |
| **4** | 12.1 ± 1.2 | 5.6 ± 0.9 |
| **3a** | 17.9 ± 1.1 | 8.6 ± 1.9 |
| **4a** | 7.4 ± 0.9 | 3.3 ± 0.9 |

same concentration, Table 4.

## 4. Conclusion

In summary, zinc (**3a**) and indium (**4a**) phthalocyanines containing chalcone cationic groups have been prepared and their photophysical and photochemical studies were investigated proving that the compounds had singlet-oxygen generating ability. When examining their photodynamic antibacterial potencies, it was noticed that these compounds exhibited a high photodynamic inhibition against *S. aureus* and *E. coli* planktonic cells with Log CFU/mL values above 9 leaving no viable bacteria cells at a very low concentration of 1.25 μM after 30 min exposition to red light (λ= 670 nm). The resultant data from experiments conducted on their most difficult treated biofilms were also impressive as these compounds **3a** and **4a** were mostly active and showed some photoactivity toward both biofilms' strains. The biofilms cell survival was estimated to be less than 3% for **3a** and **4a** after treating *S. aureus* with 100 μM whereas on *E. coli* it was generally less than 5%, following 30 min irradiation. And on the other hand, **3a** and **4a** exhibited very high PDT activity giving $IC_{50}$ values of 17.9 and 7.4 μM, respectively against MCF-7 cancer cells.

Generally, these results suggest that the reported cationic complexes in this work can highly be used as potential non-aggregated antibacterial biofilms and anticancer photosensitizers.

We trust that this study provides new and more efficient photosensitizers for use in photodynamic therapy-based bacterial and cancer treatment. Therefore, for future studies, to understand the selectivity and/or mechanism of this type of cationic phthalocyanines, we recommend a deep study of the structure-activity relationships of these molecules and different kinds of bacterial biofilms and cancer strains.

## CRediT authorship contribution statement

**Yolande Ikala Openda:** Writing – original draft, Methodology, Investigation, Funding acquisition, Conceptualization. **Balaji Babu:** Methodology, Data curation. **Tebello Nyokong:** Writing – review & editing, Supervision, Resources, Funding acquisition.

## Declaration of Competing Interest

There are no conflicts of interest to declare.

## Acknowledgments

This work was supported by the Department of Science and Technology (DST) Innovation and National Research Foundation (NRF), South Africa through DST/NRF South African Research Chairs Initiative for Professor of Medicinal Chemistry and Nanotechnology (UID 62620), Rhodes University, the Organization for Women in Science for the Developing World (OWSD) and Swedish International Development Cooperation Agency (Sida).

## Supplementary materials

Supplementary material associated with this article can be found, in the online version, at doi:10.1016/j.pdpdt.2022.102863.

## References


[1] Á. Juarranz, P. Jaén, F. Sanz-Rodríguez, J. Cuevas, S. González, Photodynamic therapy of cancer: basic principles and applications, Clin. Transl. Oncol. 10 (2008) 148–154, https://doi.org/10.1007/s12094-008-0172-2.

[2] D.E.J.G.J. Dolmans, D. Fukumura, R.K. Jain, Photodynamic therapy for cancer, Nat. Rev. Cancer 3 (2003) 380–387, https://doi.org/10.1038/nrc1071.

[3] A. Ahmad, A. Hayat, M. Ur Rahman, J. Khan, Phthalocyanines derivatives as control approach for antimicrobial photodynamic therapy, Am. J. Clin. Microbiol. Antimicrob. 2 (2019) 1041.

[4] P. Agostinis, K. Berg, K.A. Cengel, T.H. Foster, A.W. Girotti, S.O. Gollnick, S. M. Hahn, M.R. Hamblin, A. Juzeniene, D. Kessel, M. Korbelik, J. Moan, P. Mroz, D. Nowis, J. Piette, B.C. Wilson, J. Golab, Photodynamic therapy of cancer: an update, CA Cancer J Cli 61 (2011) 250–281, https://doi.org/10.3322/caac.20114.

[5] M. Wainwright, T. Maisch, S. Nonell, K. Plaetzer, A. Almeida, G.P. Tegos, M. R. Hamblin, Photoantimicrobials are we afraid of the light? Lancet Infect. Dis. 17 (2017) 49–55, https://doi.org/10.1016/S1473-3099(16)30268-7.

[6] Y. Liu, R. Qin, S.A.J. Zaat, E. Breukink, M. Heger, Antibacterial photodynamic therapy: overview of a promising approach to fight antibiotic-resistant bacterial infections, J. Clinical Translat. Res. 1 (2015) 140–167. PMCID: PMC6410618 PMID: 30873451.

[7] Y. Qing, H. Xuan, Z. Tian, W. Weili, Y. Dongliang, S. Jinjun, D. Xiaochen, Near-infrared Aza-BODIPY dyes through molecular surgery for enhanced photothermal and photodynamic antibacterial therapy, In: *Chemical Research in Chemical Universities*, Eds. J. Yu, D. Wang, Jilin University and Springer: Changchun, 37 (2021) 951–959. doi:10.1007/s40242-021-1190-7.

[8] C.M. Moore, D. Pendse, M. Emberton, Photodynamic for prostate cancer- a review of current status and future promise, Nat. Rev. Cancer 3 (2003) 380–387.

[9] M.J. Lamberti, N.B.R. Vittar, V.A. Rivarola, Breast cancer as photodynamic therapy target: enhanced therapeutic efficiency by overview of tumor complexity, World J. Clin. Oncol. 5 (2014) 901–907, https://doi.org/10.5306/wjco.v5.i5.901.

[10] D. Chen, Q. Xu, W. Wang, J. Shao, W. Huang, X. Dong, Type I photosensitizers revitalizing photodynamic oncotherapy, Small 17 (2021), 2006742, https://doi.org/10.1002/smll.202006742.

[11] Z. Malik, J. Hanania, Y. Nitzan, Bactericidal effects of photoactivated porphyrins_ an alternative approach to antimicrobial drugs, J. Photochem. Photobiol. 5 (1990) 281–293.

[12] Y.I. Openda, R. Matshitse, T. Nyokong, A search for enhanced photodynamic activity against *Staphylococcus aureus* planktonic cells and biofilms: the evaluation of phthalocyanine-detonation nanodiamonds-Ag nanoconjugates, Photochem. Photobiol. Sci. 19 (2020) 1442, https://doi.org/10.1039/D0PP00075B.

[13] I.C.J. Zanin, J.A. Brugnera, R.B. Goncalves, In vitro study of bactericidal effect of low level laser therapy in the presence of photosensitizer on cariogenic bacteria, Laser Dent 2 (2002) 154–161, https://doi.org/10.1093/jac/dki232.

[14] M. Sharma, L. Visai, F. Bragheri, I. Cristiani, P.K. Gupta, d.P. Speziale, Toluidine blue-mediated photodynamic effects on staphylococcal biofilms, Antimicrob. Agents Chemother. 52 (2008) 299–305, https://doi.org/10.1128/AAC.00988-07.

[15] M. Wilson, T. Burns, J. Pratten, Killing of *Streptococcus sanguis* in biofilms using a light-activated antimicrobial agent, J. Antimicrob. Chemother. 37 (1996) 377–381, https://doi.org/10.1093/jac/37.2.377.

[16] T.P. Paulino, K.F. Ribeiro, G.J. Thedei, A.C. Tedesco, P. Ciancaglini, Use of hand held photopolymerizer to photoinactivate Streptococcus mutans, Arch. Oral Biol. 50 (2005) 353–359, https://doi.org/10.1016/j.archoralbio.2004.09.002.

[17] S.M. Banerjee, S. El-Sheikh, A. Malhotra, C.A. Mosse, S. Parker, N.R. Williams, A. J. MacRobert, R. Hamoudi, S.G. Bown, M.R.S. Keshtgar, Photodynamic therapy in primary breast cancer, J. Clin. Med. 9 (2020) 483, https://doi.org/10.3390/jcm9020483.

[18] A. Wang, R. Zhou, L. Zhou, K. Sun, J. Jiang, S. Wei, Positively charged phthalocyanine-arginine conjugates as efficient photosensitizer for photodynamic therapy, Bioorg. Med. Chem. 25 (2017) 1643–1651, https://doi.org/10.1016/j.bmc.2017.01.029.

[19] A. Magadla, B. Babu, J. Mack, T. Nyokong, Positively charged styryl pyridine substituted Zn(II) phthalocyanines for photodynamic therapy and photoantimicrobial chemotherapy: effect of the number of charges, Dalton Trans. 50 2 (021) (2022) 9129–9136, https://doi.org/10.1039/D1DT01047F.

[20] F. Aribi, C. Vey, D. Topkaya, S.T. Kostakoglu, J. Fournier-dit-Chabert, S. I. Büyükekşi, G.C. Taşkın, S. Alpugan, F. Albrieux, A.G. Gürek, M. Cucca, D. Atilla K.Bennis, V. Ahsen, S. Ducki, F. Dumoulin, Phthalocyanine-chalcone conjugates, J. Porphyrins Phthalocyanines 20 (2016) 497–504.

[21] B. Srinivasan, T.E. Johnson, C. Xing, Chalcone-based inhibitors against hypoxia-inducible factor 1-structure activity relationship studies, Bioorg. Med. Chem. Lett. 21 (2011) 555–557, https://doi.org/10.1016/j.bmcl.2010.10.063.

[22] Y.I. Openda, T. Nyokong, Enhanced photo-ablation effect of positively charged phthalocyanines-detonation nanodiamonds nanoplatforms for the suppression of *Staphylococcus aureus* and *Escherichia coli* planktonic cells and biofilms, J. Photochem. Photobiol. A: Chem. 411 (2021), 113200, https://doi.org/10.1016/j.jphotochem.2021.113200.

[23] Y. Zhang, K. Zheng, Z. Chen, J. Chen, P. Hu, L. Cai, Z. Iqbal, M. Huang, Rapid killing of bacteria by a new type of photosensitizer, Appl. Microbiol. Biotechnol. 101 (2017) 4691–4700.

[24] A. Warrier, N. Mazumder, S. Prabhu, K. Satyamoorthy, T.S. Murali, Photodynamic therapy to control microbial biofilms, Photodiagnosis Photodyn. Ther. 33 (2021), 102090, https://doi.org/10.1016/j.pdpdt.2020.102090.

[25] H. Wang, L. Li, P. Wang, X. Wang, K. Zhang, Q. Liu, comparison of photodynamic treatment produced cell damage between human breast cancer cell MCF-7 and its multidrug resistance cell, Photodiag. Photodyn. Ther. 16 (2016) 1–8.

[26] M. Ambroz, A. Beeby, A.J. McRobert, M.S.C. Simpson, R.K. Svensen, D. Phillips, Preparative, analytical and fluorescence spectroscopic studies of sulfonated aluminium phthalocyanine photosensitizers, J. Photochem, Photobiol. B: Biol. 9 (1991) 87–95.

[27] S. Bilginer, H.I. Gul, E. Mete, U. Das, H. Sakagami, N. Umemura, J.R. Dimmock, 1-(3-Aminomethyl-4-hydroxyphenyl)-3-pyridinyl-2-propen-1-ones: a novel group of tumour-selective cytotoxins, J. Enzyme Inhib. Med. Chem. 28 (2013) 974–980.

[28] M. Demirol, L.S.E. Çalıskan, F. Biryan, K. Koran, F. Yakuphanoglu, Synthesis and photodiode properties of chalcone substituted metallo-phthalocyanine, J. Mol. Struct. 1219 (2020), 128571.

[29] X.-.S. Li, J. Guo, J.-.J. Zhuang, B.-.Y. Zheng, M.-.R. Ke, Jian-Dong Huang, Highly positive-charged zinc(II) phthalocyanine as non-aggregatedand efficient antifungal photosensitizer, Bioorg. Med. Chem. Lett. 25 (2015) 2386–2389, https://doi.org/10.1016/j.bmcl.2015.04.004.

[30] A. Ogunsipe, J.Y. Chen, T. Nyokong, Photophysical studies of zinc (II) phthalocyanine-effects of substituents and solvents, New J. Chem. 28 (2004) 822–827, https://doi.org/10.1039/B315319C.

[31] T. Nyokong, E. Antunes, in K. M. Kadish, K.M. Smith, R. Guilard (Eds), Photochemical and photophysical properties of metallophthalocyanines, The Handbook of Porphyrin Science World Scientific Singapore 2010, 247–349. doi:10.1142/9789814307246_0006.

[32] E.A. Lukyanets, V.N. Nemykin, The key role of peripheral substituents in the chemistry of phthalocyanines and their analogs, J. Porphyrins Phthalocyanines 14 (2010) 1–40, https://doi.org/10.1142/S1088424610001799.

[33] H. Karaca, Z. Kurt, S. Sezer, Synthesis of novel chalcone substituted metallophthalocyanines: electrochemistry, Spectro-electrochemistry, and catalytic oxidation of 2-mercaptoethanol, JOTCSA 5 (2018) 701–718, https://doi.org/10.18596/jotcsa.351559.

[34] F. Özen, A. Günel, A. Baran, DNA-binding, enzyme inhibition, and photochemical properties of chalcone containing metallophthalocyanine compounds, Bioorg. Chem. 81 (2018) 71–78, https://doi.org/10.1016/j.bioorg.2018.08.002.

[35] E. Gürel, M. Pişkin, S. Altun, Z. Odabaş, M. Durmuş, Synthesis, characterization and investigation of the photophysical and photochemical properties of highly soluble novel metal-free, zinc(II), and indium(III) phthalocyanines substituted with 2,3,6-trimethylphenoxy moieties, Dalton Trans 44 (2015) 6202–6211, https://doi.org/10.1039/C5DT00304K.

[36] M. Durmus, V. Ahsen, Water-soluble cationic gallium (III) and indium (III) phthalocyanines for photodynamic therapy, J. Inorg. Biochem 104 (2010) 297–309, https://doi.org/10.1016/j.jinorgbio.2009.12.011.

[37] L.W. Wijayanti, R.T. Swasono, W. Lee, J. Jumina, Synthesis and evaluation of chalcone derivatives as novel sunscreen agent, Molecules 26 (2021) 2698, https://doi.org/10.3390/molecules26092698.

[38] T. Nyokong, Effects of substituents on the photochemical and photophysical properties of main group metal phthalocyanines, Coord. Chem. Rev 251 (2007) 1707–1722. DOI10.1016/j.ccr.2006.11.011.

[39] N. Kahriman, Y. Ünver, H.T. Akçay, A.D. Gülmez, M. Durmus, I. Degirmencioglu, Photophysical and photochemical study on novel axially chalcone substituted silicon (IV) phthalocyanines, J. Mol. Struct. 1200 (2020), 127132, https://doi.org/10.1016/j.molstruc.2019.127132.

[40] M. Durmus, Photochemical and photophysical characterization, in: T. Nyokong, V. Ahsen (Eds.), Photosensitizers in Medicine, Environment and Security, Springer, Dordrecht, Heidelberg, London, New York, 2012, p. 135e266.

[41] M. Miletin, P. Zimcik, V. Novakova, Photodynamic properties of aza-analogues of phthalocyanines, Photochem. Photobiol. Sci. 17 (2018) 1749–1766, https://doi.org/10.1039/C8PP00106E.

[42] L. Wu, C. Huang, P.B. Emery, A.C. Sedgwick, S.D. Bull, X.P. He, H. Tian, J. Yoon, J. L. Sessler, T.D. James, Förster resonance energy transfer (FRET)-based small-molecule sensors and imaging agents, Chem. Soc. Rev. 49 (2020) 5110, https://doi.org/10.1039/C9CS00318E.

[43] V. Çakır, M. Goksel, M. Durmus, Z. Biyiklioglu, Synthesis and photophysicochemical properties of novel water soluble phthalocyanines, Dyes Pigments 125 (2016) 414–425.

[44] M.U. Rasheed, N. Thajuddin, P. Ahamed, Z. Teklemariam, K. Jamil, Antimicrobial drug resistance in strains of *Escherichia coli* isolated from food sources, Rev. Inst. Med. Trop. 56 (2014) 341–346, https://doi.org/10.1590/s0036-46652014000400012.

[45] T.J. Foster, Antibiotic resistance in staphylococcus aureus. Current status and future prospects, FEMS Microbiol. Rev. 41 (2017) 430–449, https://doi.org/10.1093/femsre/fux007.

[46] A. Minnock, D.I. Vernon, J. Schofield, J. Griffiths, J.H. Parish, S.B. Brown, Mechanism of uptake of a cationic water-soluble pyridinium zinc phthalocyanine across the outer membrane of *Escherichia coli*, Antimicrob. Agents Chemother. 44 (2000) 522–527, https://doi.org/10.1128/aac.44.3.522-527.2000.

[47] Z. Biyiklioglu, I. Ozturk, T. Arslan, A. Tunçel, K. Ocakoglu, M. H.-Limoncu, F. Yurt, Synthesis and antimicrobial photodynamic activities of axially {4-[(1E)-3-*oxo*-3-(2-*thienyl*)*prop*-1-*en*-1-*yl*]phenoxy} groups substituted silicon phthalocyanine, subphthalocyanine on Gram-positive and Gram-negative bacteria, Dyes Pigments 166 (2019) 149–158, https://doi.org/10.1016/j.dyepig.2019.03.010.

[48] F.F. Sperandio, Y.-.Y. Huang, M.R. Hamblin, Antimicrobial photodynamic therapy to kill gram-negative bacteria, Recent Pat. Antiinfect. Drug Discov. 8 (2013) 108–120, https://doi.org/10.2174/1574891x113089990012.

[49] H. Abrahamse, M.R. Hamblin, New photosensitizers for photodynamic therapy, Biochem. J. 473 (2016) 347–364, https://doi.org/10.1042/BJ20150942.

[50] B. Babu, R.C. Soy, J. Mack, T. Nyokong, Non-aggregated lipophilic water-soluble tin porphyrins as photosensitizers for photodynamic therapy and photodynamic antimicrobial chemotherapy, New J. Chem. 44 (2020) 11006.

[51] T. Mosmann, Rapid colorimetric assay for cellular growth and survival: application to proliferation and cytotoxicity assays, J. lmmunol. Methods 65 (1983) 55–63, https://doi.org/10.1016/0022-1759(83)90303-4.

[52] V.D. Straten, V. Mashayekhi, H. de Bruijn, S. Oliveira, D.J. Robinson, Oncologic photodynamic therapy: basic principles, current clinical status, and future directions, Cancers (Basel) 9 (2017) 19, https://doi.org/10.3390/cancers9020019.